Anisotropic Regularization for Inverse Problems with Application to the Wiener Filter with Gaussian and Impulse Noise

Micha Feigin and Nir Sochen

School of Mathematics, Tel Aviv University
michf@post.tau.ac.il, sochen@post.tau.ac.il

Abstract. Most inverse problems require a regularization term on the data. The classic approach for the variational formulation is to use the L_2 norm on the data gradient as a penalty term. This however acts as a low pass filter and thus is not good at preserving edges in the reconstructed data.

In this paper we propose a novel approach whereby an anisotropic regularization is used to preserve object edges. This is achieved by calculating the data gradient over a Riemannian manifold instead of the standard Euclidean space using the Laplace-Beltrami approach. We also employ a modified fidelity term to handle impulse noise.

This approach is applicable to both scalar and vector valued images. The result is demonstrate via the Wiener filter with several approaches for minimizing the functional including a novel GSVD based spectral approach applicable to functionals containing gradient based features.

1 Introduction

Handling degraded images, both due to blur and noise, is a practical reality in any imaging field. The common image degradation model is

$$I = I_0 * h + n \tag{1}$$

where I, the observed image, is the result of a convolving the input image (or ideal image) I_0 with some blurring kernel h. The result is then summed with additive noise n. This is a common model for any system that contains a lens and sensor. Both the blur and noise are a combination of several processes. Some typical causes for image blue are out of focus images, motion blur due to an unstable camera and/or object and a low pass filter resulting from the finite aperture and anti aliasing filter on the sensor. Noise can result from the sensor and amplifier due to low light, heat, dead pixels and background radiation or from memory and communication corruption. Each of these processes has it's own typical blur kernel and noise distribution statistics [1, 2].

A direct naive approach to handle the blur can be given using a spectral (Fourier) approach manipulation of the degradation model equation. To see the difficulty though, look at the Fourier transform of this equation $\hat{I} = \hat{I}_0 \cdot \hat{h} + \hat{n}$

X.-C. Tai et al. (Eds.): SSVM 2009, LNCS 5567, pp. 319–330, 2009.

(where the hat notation denotes the Fourier transform). This transforms the convolution into a multiplication which allows for an easy rearrangement of the the equation. Extracting $\hat{I}_0$ gives us $\hat{I}_0 = \left(\hat{I} - \hat{n}\right)/\hat{h}$. Any L_2 kernel h will decay to zero at infinity. This results with a divide by zero issue at least for high frequencies. Add to that the issue that the SNR usually drops at these frequencies, which makes this procedure very sensitive to noise.

One solution is this case is the Wiener filter [3], which can be derived from the standard variational formulation for ill posed inverse problems by adding prior knowledge (or assumptions) via an additional penalty term to the reconstruction. That is to minimize an energy functional of the form

$$S(I_0) = \underbrace{\|I_0 * h - I\|}_{\text{fidelity term}} + \underbrace{\mu \|\Phi(I_0)\|}_{\text{penalty}}. \tag{2}$$

Here Φ is some function of the parameter I_0 that imposes the assumptions on the model. A common constraint term is $\Phi(I_0) = \nabla I_0$ which penalizes high frequencies as these are often the source of instability. The side effect of this constraint is that while high frequency noise is reduced in the reconstruction, edge detail is lost as well as is demonstrated in Fig. 1.

(a) Original Image (b) Degraded Input (c) $\mu = 5 \cdot 10^{-4}$ (d) $\mu = 5 \cdot 10^{-5}$

Fig. 1. Edge preservation vs. Noise suppression with the Wiener filter. The input image 1(a) is degraded using Gaussian white noise 1(b). The results show the difference between preferring noise suppression 1(c) to edge preservation 1(d).

This functional is often minimized under the L_2 norm which is appropriate for Gaussian noise. This is mainly due to the fact that the resulting Euler Lagrange equations are linear and are thus (relatively) easy to solve. That is, the classic Wiener filter functional based on the L_2 norm

$$S(I_0) = \|I_0 * h - I\|_{L_2}^2 + \|\nabla I_0\|_{L_2}^2 = \int |I_0 * g - I|^2 + |\nabla I_0|^2 \, dA\,. \tag{3}$$

results with the following Euler Lagrange equations (see [4] for the derivation of the Euler Lagrange formulation of the convolution)

$$-h(-\bar{x}) * (h(\bar{x}) * I_0 - I) - \mu \Delta I_0 = 0\,. \tag{4}$$

Here $\bar{x}$ is the coordinate vector $\bar{x} = (x, y)$ for the two dimensional case. This can be solved as before by applying the Fourier transform, which results with

$$\hat{h}(-\omega) \cdot \left(\hat{h}(\bar{\omega}) \cdot \hat{I}_0 - \hat{I} \right) + \mu |\bar{\omega}|^2 \hat{I}_0 = 0 \tag{5}$$

where $\bar{\omega} = (\omega_x, \omega_y)$ is the frequency vector for the resulting frequencies along the x and y axes respectively. Now, assuming that the convolution kernel is real we can use the identity $\hat{h}(-\omega) = \hat{h}^*(\omega)$ (where h^* is the conjugate of h) to rewrite the equation as

$$\hat{I}_0 = \frac{\hat{h}^*(\omega)}{\left|\hat{h}(\omega)\right|^2 + \mu |\omega|^2} \hat{I}\,. \tag{6}$$

Despite being easy to solve, there are two main issues with the L_2 norm approach, both for the constraint and the fidelity term.

The first issue is that it fails to preserve object boundaries (Fig. 1). The main reason is the penalty term that penalizes high frequencies. As the fidelity term is also L_2 it does little to alleviate this problem.

The second issue is that the fidelity term is designed to handle Gaussian noise and behaves poorly in the presence of impulse noise

One solution to both these issues is to use the L_1 or total variation (TV) norm [5,6,7]. When used for the fidelity term it improves behavior with impulse noise. For the constraint it improves edge preservation. For the functional

$$S(I_0) = \|I_0 * h - I\|_{TV} + \mu \|\nabla I_0\|_{TV} = \int |I_0 * h - I| + \mu |\nabla I_2|\, dA \tag{7}$$

the resulting Euler-Lagrange equations are

$$-h(-\bar{x}) * \frac{h(\bar{x}) * I_0 - I}{|h(\bar{x}) * I_0 - I|} - \mu \mathrm{div}\left(\frac{\nabla I}{|\nabla I|} \right) = 0\,. \tag{8}$$

Unfortunately though the solution of which is unstable. One approach to improve on this is to use an augmented TV norm [5]

$$S(I_0) = \int \sqrt{(I_0 * h - I)^2 + \eta} + \mu \sqrt{|\nabla I_0|^2 + \eta} dA \tag{9}$$

with $0 < \eta \ll 1$. The resulting modified Euler-Lagrange equation are

$$-h(-\bar{x}) * \frac{h(\bar{x}) * I_0 - I}{\sqrt{(h(\bar{x}) * I_0)^2 + \eta}} - \mu \mathrm{div}\left(\frac{\nabla I}{\sqrt{|\nabla I|^2 + \eta}} \right) = 0\,. \tag{10}$$

This greatly improves the response of the fidelity term to impulsive noise, but not so much for the edge preservation of the constraint. It also doesn't account explicitly for the edges in the image.

Other approaches include using Mumford-Shah like techniques of edge detection into the functional [4], weighing the Laplacian based on edge detection [8], Perona-Malik like regularizers [9], maximal likelihood estimators [10], certainty maps [11] and channel pairing on color images [12].

We propose two novelties in this paper. The first is to combine the augmented L_1 norm on the fidelity term for handling impulse noise with anisotropic regularization based on the Laplace Beltrami operator for edge preservation. This is achieved by keeping the L_2 norm of the gradient, however this is calculated over a Riemannian manifold instead of the standard Euclidean space using a Laplace-Beltrami approach [13]. When combined with the augmented TV norm (9), this approach also produces exceptional results for impulsive noise (Sec. (4))

The second is the use of the GSVD (generalized singular value decomposition) for the minimization of functionals that employ a gradient based penalty term. It's direct contribution is the ability easily minimize non-local operators and functionals defined on non square domains where the Fourier transform is inapplicable. For isotropic operators it can be very efficient as the decomposition needs to be calculated once only off line.

One interesting point to both these approaches is the relation to other frameworks. In particular it enables to better understand the relation to sparse representation and K-SVD [14].

It is important to note that both these ideas are easily applicable to general ill posed inverse problems over general feature spaces, and specifically for this case, also for color images [15] and textures [16].

The rest of this paper is organized as follows: Sec. 2 discusses the anisotropic approach. Sec. 3 discusses several approaches to minimizing the functional, including a novel approach using the GSVD. Sec. 4 shows some results of the method.

2 Anisotropic Regularization for the Wiener Filter

The problem with edge preservation lies with the gradient based penalty term. In the Euler-Lagrange equations it manifests as a Laplacian that acts as a low pass filter. In order to correctly formulate the anisotropic penalty term, we start with the Euler Lagrange equation for the Wiener filter

$$-h\left(-x\right)*\left(h\left(x\right)*I_0-I\right)-\mu\Delta I_0=0 \tag{11}$$

and replace the Laplacian with an anisotropic operator, namely the Laplace-Beltrami operator [13] resulting with

$$-h\left(-x\right)*\left(h\left(x\right)*I_0-I\right)-\mu\Delta_g I_0=0\,. \tag{12}$$

The Laplace Beltrami operator is defined as

$$\Delta_g I=\frac{1}{\sqrt{g}}\mathrm{div}\left(\sqrt{g}G^{-1}\nabla I\right) \tag{13}$$

where for the gray-scale case

$$G=\begin{pmatrix}1+I_x^2 & I_xI_y\\ I_xI_y & 1+I_y^2\end{pmatrix},\quad g=\det\left(G\right)\,. \tag{14}$$

What this does is apply the Laplacian diffusion operator, but instead of applying it under the standard Euclidean norm, it is applied over the image manifold [13].

This means that we are looking at the image as a two dimensional manifold in three dimensional space for gray scale images and in 5 dimensional space for color images. When applying the diffusion operator, distance between pixels is measured over this manifold so the distance takes into account not only spatial offset but also intensity offset. The result is that pixels on different side of an edge are farther apart than pixels on the same homogeneous region and the edges act as insulators so that image data doesn't flow across edges.

This can be extended to color images by applying the diffusion on a per-channel basis, that is for each channel I^i the process is $\Delta_g I^i = \frac{1}{\sqrt{g}} \operatorname{div}\left(\sqrt{g} G^{-1} \nabla I^i\right)$ with

$$G = \begin{pmatrix} 1 + \sum_i \left(I_x^i\right)^2 & \sum_i I_x^i I_y^i \\ \sum_i I_x^i I_y^i & 1 + \sum_i \left(I_y^i\right)^2 \end{pmatrix} . \tag{15}$$

The metric itself takes into account all the channels coupling them in the final process to remove misalignment of the edges across the different channels. Note that the image channels can be color channels such as RGB, CMY or more general features such as textures [16]).

When extending the functional to handle impulse noise using the augmented L_1 fidelity term, the Euler-Lagrange equations become instead

$$-h\left(-\bar{x}\right) * \frac{h\left(\bar{x}\right) * I_0 - I}{\sqrt{\left(h\left(\bar{x}\right) * I_0\right)^2 + \eta}} - \mu \Delta_g I = 0 . \tag{16}$$

3 Finding the Minimizer

There are several approaches to minimizing the resulting functional. We already have the Euler-Lagrange equations, i.e Eq. (12) and 16.

Using the direct Fourier space approach, even for the L_2 fidelity term, is not applicable here since the Fourier transform doesn't diagonalize the Laplace-Beltrami operator. A different relatively simple direct approach approach is to use the gradient descent equations

$$\frac{\partial}{\partial t} I_0 = h\left(-\bar{x}\right) * \frac{h\left(\bar{x}\right) * I_0 - I}{\sqrt{\left(h\left(\bar{x}\right) * I_0\right)^2 + \eta}} + \mu \Delta_g I \tag{17}$$

For the L_2 fidelity term there are two other spectral approaches that can be applied here, and eigen transform and the GSVD. The advantage of these among other things is that they provide a direct solution and thus prove the existence of the minimizer, same as for the standard Wiener filter.

Proving the existence of a minimizer for the proposed Tikhonov functional is much more difficult and beyond the scope of this paper, but can be done using similar lines to those taken in [5].

3.1 The Laplace-Beltrami Eigen-Space

We can use the same approach implemented in [17] to diagonalize the Laplace-Beltrami operator. The problem is that the Eigenvectors of the Laplace-Beltrami

operator don't convert the convolution into a multiplication, so we need to combine this approach with the Fourier transform.

We start with the Euler-Lagrange equations for the anisotropic Wiener filter, Eq. (12). If we linearize the Laplace Beltrami operator by fixing the metric, it becomes a self adjoint negative (semi) definite operator and thus it's eigenspace is a bases to the function space under the L_2 norm. Insert into this equation the eigen decomposition of the image using this eigen space

$$I_0 = \sum_i c_i^0 \phi_i, \quad I = \sum_i c_i \phi_i \tag{18}$$

This produces

$$h(-x) * \left(h(x) * \sum_i c_i^0 \phi_i - \sum_i c_i \phi_i \right) + \mu \sum_i \lambda_i c_i^0 \phi_i = 0 \tag{19}$$

which after rearrangement gives

$$\sum_i c_i^0 h(-x) * h(x) * \phi_i + \mu \lambda_i c_i^0 \phi_i = \sum c_i h(-x) * \phi_i \,. \tag{20}$$

Now, to handle the convolution, apply the Fourier transform

$$\sum_i -\hat{h}^* \cdot \hat{h} \cdot c_i^0 \hat{\phi}_i + \mu \lambda_i c_i^0 \hat{\phi}_i = -\sum_i c_i \hat{h}^* \hat{\phi}_i \tag{21}$$

which can be rewritten as

$$\sum_i c_i^0 \left(\left| \hat{h} \right|^2 - \mu \lambda_i \right) \hat{\phi}_i = \sum_i c_i \hat{h}^* \hat{\phi}_i \,. \tag{22}$$

This is a linear set of equations of the form $A\tilde{I}_0 = B\tilde{I}$. Here $\tilde{I} = (c_i)$ and $\tilde{I}_0 = \left(c_i^0\right)$ are the coefficient vectors in the Laplace-Beltrami eigen-space. This is a system of equations needs to be solved for $\tilde{I}_0$. Using these coefficients the ideal image I_0 can be reconstructed.

For a full solution this needs to be combined with fixed point iterations updating the metric, although it is stable with respect to the flow so in effect this is rarely need.

There are two things to note here. First, the coefficients of I decay rather quickly so we can truncate $\tilde{I}$ and thus not calculate the right hand side of B. The same assumption can be made for $\tilde{I}_0$ and thus for A.

3.2 Using the GSVD

Consider an energy functional with two linear operators L_a and L_b using the L_2 norm

$$S(f) = \int |L_a f|^2 + \mu |L_b f|^2 \, dA \,. \tag{23}$$

Assuming that these operators can be discretized as matrices A and B respectively this can written as equations with v a vector representation of the function f

$$S(v) = \|Av\|^2 + \mu \|Bv\|^2 . \tag{24}$$

The two matrices A and B have a joint diagonalization based on the general singular value decomposition (GSVD) of the form [18]

$$A = U\Sigma_1 X^T, \quad B = V\Sigma_2 X^T \tag{25}$$

with U and V unitary matrices and Σ_1 and Σ_2 positive diagonal (not necessarily square). U and V must have the same number of columns but not necessarily the same number of rows (this last property we will need later on). Thus Eq. (24) can be rewritten as

$$S(v) = \left\|U\Sigma_1 X^T v\right\|_{L_2}^2 + \mu \left\|V\Sigma_2 X^T v\right\|_{L_2}^2 . \tag{26}$$

Now, we can substitute $\tilde{v} = X^T v$ to construct a functional in $\tilde{v}$. Also note that the L_2 norm is invariant to unitary transformations, thus this functional is equivalent to

$$S(\tilde{v}) = \|\Sigma_1 \tilde{v}\|_{L_2}^2 + \mu \|\Sigma_2 \tilde{v}\|_{L_2}^2 . \tag{27}$$

This new functional can be minimized according to $\tilde{v}$ resulting with

$$\Sigma_1^T \Sigma_1 \tilde{v} + \mu \Sigma_2^T \Sigma_2 \tilde{v} = 0 \tag{28}$$

We would like to do something similar with the Wiener-Filter formulation. The problem is that the gradient operator can not be discretized as a matrix operator since it takes a function and returns a vector. Luckily, what we need is an operator operating on I such that the norm would be equal to that of the gradient. For the L_2 case this can be achieved as follows

$$\begin{aligned} S(I_0) &= \int |h * I_0 - I|^2 + \mu |\nabla I_0|^2 \, dA \\ &\Rightarrow \|HI_0 - I\| + \left\| \begin{pmatrix} D_x \\ D_y \end{pmatrix} I_0 \right\|_{L_2}^2 = \|HI_0 - I\|_{L_2}^2 + \|DI_0\|_{L_2}^2 \end{aligned} \tag{29}$$

where H is the convolution matrix (which is block cyclic but not cyclic in the 2D case) and $D = \binom{D_x}{D_y}$ is the matrix resulting from stacking the matrix for the derivative in the x direction and the one for the derivative in the y direction. For the L_2 case we get

$$\left\| \begin{pmatrix} D_x \\ D_y \end{pmatrix} I_0 \right\|_{L_2}^2 = \|D_x I_0\|_{L_2}^2 + \|D_y I_0\|_{L_2}^2 = \|\nabla I_0\|_{L_2}^2 . \tag{30}$$

Now we can use the fact that the GSVD can be applied to matrices with a different number of rows to diagonalize this equation

$$H = U\Sigma_1 X^T, \quad D = V\Sigma_2 X^T \tag{31}$$

Using this we can do the same procedure as before

$$\|HI_0 - I\|_{L_2}^2 + \|DI_0\|_{L_2}^2 \Rightarrow \left\|U\Sigma_1 X^T I_0 - I\right\|_{L_2}^2 + \left\|V\Sigma_2 X^T I_0\right\|_{L_2}^2 \tag{32}$$

and again based on U and V being unitary and substituting $\tilde{I}_0 = X^T I_0$ and $\tilde{I} = U^{-1}I = U^T I$ results with

$$S\left(\tilde{I}_0\right) = \left\|\Sigma_1\tilde{I}_0 - \tilde{I}\right\|_{L_2}^2 + \left\|\Sigma_2\tilde{I}_0\right\|_{L_2}^2 \tag{33}$$

this can be minimized according to $\tilde{I}_0$ to produce

$$\Sigma_1^T\left(\Sigma_1\tilde{I}_0 - \tilde{I}\right) + \Sigma_2^T\Sigma_2\tilde{I}_0 = 0 \tag{34}$$

or after rearrangement and back-substitution

$$I = X^{-T}\left(\Sigma_1^T\Sigma_1 + \mu\Sigma_2^T\Sigma_1\right)^{-1}\Sigma_1^T U^T I_0\,. \tag{35}$$

Note that $\Sigma_1^T\Sigma_1 + \mu\Sigma_2^T\Sigma_1$ is a diagonal matrix and thus easy to invert (in fact for $\mu = 1$ it is the identity matrix).

To apply the same idea to the anisotropic case, we need to formulate the prior to the Laplace-Beltrami operator as a gradient over a manifold instead. The operator is the minimizer of the following symmetric positive definite

$$\int \nabla I^T G^{-1}\nabla I\,\sqrt{g}d^m\sigma = \int \|D_g\nabla I\|^2\,d^m\sigma, \quad \sqrt{g}G^{-1} = D_g^2 \tag{36}$$

and the discrete formulation for the anisotropic derivative matrix D_g (which replaces D in Eq. 29) can be found via an eigen decomposition of the matrix $\sqrt{g}G^{-1}$

$$D_g = A\begin{pmatrix}D_x\\D_y\end{pmatrix} = \begin{pmatrix}\frac{I_x^2+\sqrt{1+I_x^2+I_y^2}I_y^2}{\left(I_x^2+I_y^2\right)\sqrt[4]{1+I_x^2+I_y^2}}D_x + \frac{I_xI_y\left(1-\sqrt{1+I_x^2+I_y^2}\right)}{\left(I_x^2+I_y^2\right)\sqrt[4]{1+I_x^2+I_y^2}}D_y\\ \frac{I_xI_y\left(1-\sqrt{1+I_x^2+I_y^2}\right)}{\left(I_x^2+I_y^2\right)\sqrt[4]{1+I_x^2+I_y^2}}D_x + \frac{I_y^2+\sqrt{1+I_x^2+I_y^2}I_x^2}{\left(I_x^2+I_y^2\right)\sqrt[4]{1+I_x^2+I_y^2}}D_y\end{pmatrix} \tag{37}$$

One advantage of this approach is that it is applicable to non-local operators and to non square domains where the Fourier transform as applied to the original Wiener filter fails. For the isotropic case it needs to be calculated once off line as the transform is constant and thus can be very efficient for reoccurring problems (or by splitting the problem into constant sized patches as described in [17]).

4 Numerical Results

Comparing the reconstruction quality based on standard measurements alone such as SNR and PSNR doesn't do justice to the method. This is due to the fact that these values are not good assessors for edge reconstruction being L_2 based measures. Despite this and for a lack of a better objective comparison method,

we do see an improvement in the reconstruction based on these measurements. It is important to also note the subjective difference when looking at the images themselves. The biggest difference is seen near pronounced edges and textures which are much better preserved than with the standard wiener filter. This method also removes ringing (Gibbs effect) seen around strong edges and color skews in color images.

The results are cropped and zoomed to better accent the difference due to the limit of the medium.

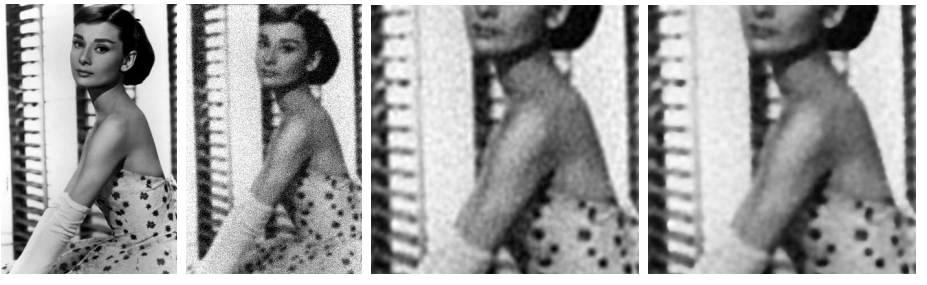

(a) Input (b) Degraded (c) Standard W.F. (d) Anisotropic W.F.

Fig. 2. Reconstruction of a gray-scale image (2(a)) degraded using a Gaussian kernel and Gaussian noise (2(b)) with standard deviation of 10%. The image is reconstructed using the standard (2(c)) and anisotropic Wiener filter (2(d)).

The first example (Fig. 2) shows the results for a gray scale image degraded by a Gaussian kernel and Gaussian noise with standard deviation of 10% (with a resulting SNR of 16.34*db*). The reconstruction for both the standard Wiener filter (2(c)) and the anisotropic version (2(d)) is done based on the L_2 fidelity term. The SNR of the reconstructed images are 20.72*db* and 21.08*db* respectively.

The anisotropic reconstruction displays less noise, especially visible in homogeneous areas such as the white background and skin. The edges in the isotropic version on the other hand display both blur (such as the back, hands and hair) and ringing around pronounced edges not appearing in the anisotropic version. This is most pronounced around the dominant edges of the back and the hair.

Figure 3 shows the results of applying the Wiener filter to an image with impulse noise (11% density, with 8.47*db* SNR). The first two examples (3(b), 3(e)) display the result of applying the standard and anisotropic Wiener filters respectively, both using the L_2 fidelity term. Despite improving SNR values (15.9*db* and 16.48*db*) the results are still rather miserable, although the anisotropic version still displays more pronounced edges (teeth, wall) as well as less noise. On the other hand, looking at the versions employing the augmented L_1 fidelity term (3(c) and 3(f)), on first look one can mistake them for the input image. Despite this the anisotropic version still displays much sharper results up close, as well as improved SNR (22.48*db* compared to 22.98*db*).

The following examples for color images show the extendability of the method to vector valued images.

(a) Input Image (b) Std. W.F. L_2 fidelity (c) Std. W.F., L_1 fidelity

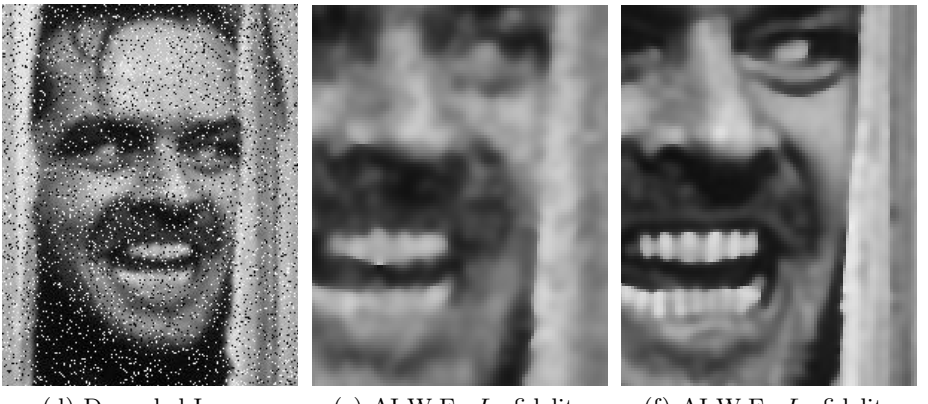

(d) Degraded Image (e) AI W.F., L_2 fidelity (f) AI W.F., L_1 fidelity

Fig. 3. Restoration of a gray scale image corrupted by impulse noise of density 0.11. Figures 3(b) and 3(e) show the reconstruction using regular and anisotropic Wiener filter with L_2 fidelity. Figures 3(c) and 3(f) show the reconstruction using the L_1 fidelity term.

Figure 4 shows the results for a color image degraded by a Gaussian kernel and Gaussian noise with a standard deviation of 10% (SNR of 16.7db). As can be seen, the anisotropic reconstruction produces sharper edges without the color shifts and ringing which is visible around sharp edges. Additionally, there is less overall noise and color shifts due to the smoothing of the noise. SNR for the isotropic case is 21.04db compared to 21.6db for the anisotropic variation.

Fig. 5 shows the results of applying both the regular and anisotropic Wiener filter, both based on the L_1 fidelity term, to a color image degraded by a Gaussian kernel and impulse noise with 11% density (SNR of 11db). The anisotropic variation shows sharper edges, better color restoration and less color skews around edge boundaries. This, like the previous results, is most pronounced around bright edges such as the teeth, eyes and wall. The SNR of the reconstruction is 20db and 23.1db for the isotropic and anisotropic varieties respectively.

(a) Degraded image (b) Standard W.F. (c) Anisotropic W.F.

Fig. 4. Color image degraded by a gaussian kernel and uncorrelated Gaussian noise (4(a)) with standard deviation of 10%. Figures 4(b) and 4(c) show the results for the standard and the anisotropic reconstruction.

(a) Degraded image (b) Std. W.F. L_1 fidelity (c) AI W.F. L_1 fidelity

Fig. 5. Color image degraded by a gaussian kernel and uncorrelated impulse noise (5(a)) with density 0.11. Figures 5(b) and 5(c) show the results for the standard and anisotropic restoration based on the L_1 fidelity term.

5 Conclusion

In this work we presented an anisotropic regularization term for inverse problems that allows to better preserve object edges while at the same time improving noise suppression. Combined with an augmented L_1 fidelity term it provides remarkable results for images corrupted by impulse noise.

References

1. Goodman, J.: Introduction to Fourier Optics. McGraw-Hill Book Company, New York (1996)
2. Jähne, B.: Digital Image Processing, 5th edn. Springer, Heidelberg (2002)

3. Gonzalez, R.C., Woods, R.E.: Digital image processing, 2nd edn. Prentice-Hall, Englewood Cliffs (2002)
4. Bar, L., Sochen, N., Kiryati, N.: Semi-blind image restoration via mumford-shah regularization. IEEE Trans. on Image Processing 15(2), 483–493 (2005)
5. Bar, L., Kiryati, N., Sochen, N.: Image deblurring in the presence of impulsive noise. Int. J. Comput. Vision 70(3), 279–298 (2006)
6. Blomgren, P., Chan, T.F.: Color tv: Total variation methods for restoration of vector-valued images. IEEE Trans. Image Processing 7, 304–309 (1998)
7. Chan, T.F., Vese, L.A.: Image segmentation using level sets and the piecewise-constant mumford-shah model. Technical Report 00-14, UCLA CAM (2000)
8. Charbonnier, P., Blanc-féraud, L., Aubert, G., Barlaud, M.: Deterministic edge-preserving regularization in computed imaging. IEEE Trans. Image Processing 6, 298–311 (1997)
9. Welk, M., Theis, D., Weickert, J.: Variational deblurring of images with uncertain and spatially variant blurs. In: Kropatsch, W.G., Sablatnig, R., Hanbury, A. (eds.) DAGM 2005. LNCS, vol. 3663, pp. 485–492. Springer, Heidelberg (2005)
10. Jalobeanu, A., Blanc-Feraud, L., Zerubia, J.: An adaptive gaussian model for satellite image deblurring. IEEE Transactions on Image Processing (4), 613–621 (2004)
11. Krajsek, K., Mester, R.: The edge preserving wiener filter for scalar and tensor valued images. In: DAGM-Symposium, pp. 91–100 (2006)
12. Kaftory, R., Sochen, N., Zeevi, Y.Y.: Variational blind deconvolution of multi-channel images. Int. J. Imaging Science and Technology 15(1), 56–63 (2005)
13. Sochen, N., Kimmel, R., Malladi, R.: A general framework for low level vision. IEEE Trans. Image Processing, Special Issue on Geometry Driven Diffusion 7, 310–318 (1998)
14. Aharon, M., Elad, M., Bruckstein, A.: The K-SVD: An algorithm for designing of overcomplete dictionaries for sparse representation. IEEE Trans. On Signal Processing 54(11), 4311–4322 (2006)
15. Kimmel, R., Malladi, R., Sochen, N.: Images as embedded maps and minimal surfaces: Movies, color, texture, and volumetric medical images. International Journal of Computer Vision 39, 111–129 (2000)
16. Sagiv, C., Sochen, N., Zeevi, Y.: Gabor features diffusion via the minimal weighted area method. In: EMMCVPR (September 2001)
17. Feigin, M., Sochen, N., Vemuri, B.C.: Efficient anisotropic α-kernels decompositions and flows. In: POCV (2008)
18. Golub, G.H., Loan, C.F.V.: Matrix computations, 3rd edn. Johns Hopkins University Press, Baltimore (1996)